RSC Advances

PAPER

View Article Online
View Journal | View Issue

Cite this: *RSC Adv.*, 2022, **12**, 9567

In-depth study of bio-oil and biochar production from macroalgae *Sargassum* sp. *via* slow pyrolysis†

Obie Farobie, *[ab] Apip Amrullah,[c] Asep Bayu,[d] Novi Syaftika,[e] Latifa Aisya Anis[b] and Edy Hartulistiyoso[ab]

Sargassum is undoubtedly one of the most predominant brown macroalgae, posing a significant disposal problem for coastal areas worldwide. The effective valorization of *Sargassum* sp. would be beneficial not only for environmental mitigation but also for producing high-value chemicals. However, the valorization of *Sargassum* sp. for bio-oil and biochar production *via* slow pyrolysis has not been well studied yet. Hence, this study aimed to conduct a comprehensive investigation into bio-oil and biochar production from *Sargassum* sp. *via* slow pyrolysis to provide valuable data for further valorization. A batch reactor was employed, and the pyrolysis of *Sargassum* sp. was conducted in a temperature range of 400–600 °C and with retention times of 10–50 min. The results showed significant compounds could be identified in bio-oil from *Sargassum* sp., including carboxylic acids, furan derivatives, aliphatic hydrocarbons, and *N*-aromatic compounds. Based on the ultimate analysis, the H/C and O/C atomic ratios of biochar were lower than the feedstock, reflecting the occurrence of dehydration and decarboxylation reactions throughout the pyrolysis. Biochar exhibited calorific values in the range of 23.12–25.89 MJ kg^{-1}, indicating it has more potential to be used as a solid fuel than low-ranked coals. Surface morphological analysis was performed by scanning electron microscopy (SEM) and showed a larger surface area in biochar than in the algal feedstock. Furthermore, a reaction model was deduced, and it was confirmed that the pyrolysis reaction obeyed the Arrhenius behaviour. Overall, the slow pyrolysis of *Sargassum* sp. provides an opportunity to obtain value-added chemicals and biochars, which could be further utilized for other applications.

Received 2nd February 2022
Accepted 14th March 2022

DOI: 10.1039/d2ra00702a

rsc.li/rsc-advances

Introduction

Our planet faces unprecedented challenges due to the rapid population growth and global development, which implies a growing energy demand. Currently, the primary energy sources used for daily life are derived chiefly from petroleum-based fossil fuels.[1] The massive consumption of petroleum fuels is exhausting these energy sources and causing environmental problems due to the augmented emissions of pollutants from burning these fuels (SO_2, NO_x, and CO_2). Even though several severe environmental challenges have been reported due to the extensive consumption of petroleum fuels, their use still serves as the most attractive and viable source for transportation fuel.[2] However, the endless consumption of fossil fuels will lead to the eventual exhaustion of petroleum sources after 2042 worldwide even without considering the projected growth of petroleum fuel consumption.[3]

Several attempts are currently underway to mitigate the energy crisis and control pollutant emissions to search for eco-friendly energy sources for future generations. One of the most promising and environmentally friendly alternative energy sources is biomass since it is abundantly available, renewable, and is considered CO_2 neutral.[4] Moreover, biomass ranks fourth as the most significant energy resource after coal, oil, and natural gas.[5] In terms of its source and utilization, biomass is categorized into four classifications: first -, second-, third, and fourth-generation. Several ways have evolved to produce biomass energy, including biochemical and thermochemical

[a]*Department of Mechanical and Biosystem Engineering, Faculty of Agricultural Engineering and Technology, IPB University (Bogor Agricultural University), IPB Darmaga Campus, Bogor, West Java 16002, Indonesia. E-mail: obiefarobie@apps.ipb.ac.id*

[b]*Surfactant and Bioenergy Research Center (SBRC), IPB University (Bogor Agricultural University), Jl. Pajajaran No. 1, IPB Baranangsiang Campus, Bogor, West Java 16144, Indonesia*

[c]*Department of Mechanical Engineering, Lambung Mangkurat University, Banjarmasin, South Kalimantan, Indonesia*

[d]*Research Center for Biotechnology, Research Organization for Life Sciences, National Research and Innovation Agency (BRIN), Jl. Raya Jakarta-Bogor KM 46 Cibinong, Bogor, West Java 16911, Indonesia*

[e]*Center for Energy Resource and Chemical Industry Technology, Research Organization for Assessment and Application of Technology, National Research and Innovation Agency (BRIN), Kawasan PUSPITEK Serpong, Tangerang Selatan, Indonesia*

† Electronic supplementary information (ESI) available: Provide result of ultimate and proximate analysis of *Sargassum* sp., chemical composition identified in bio-oil from GC/MS, band assignment for FTIR spectra of biochar at varying temperatures, typical GC/MS chromatogram of *Sargassum* sp. bio-oil. See DOI: 10.1039/d2ra00702a

conversions. Although the biochemical conversion of biomass is less energy-intensive than the thermochemical process, the biochemical route is not cost-effective since it solely needs cellulose and hemicellulose in biomass.[6] The thermochemical route of biomass into energy is considered favourable due to its more efficient and cost-effective process.[7] The thermochemical route of biomass into energy can be performed by liquefaction,[8,9] gasification,[10–13] and pyrolysis.[14,15] Among the thermochemical processes, the most common method for biomass conversion into valuable chemicals and biofuels is pyrolysis owing to its energy-efficient and economical nature.[16] Basically, pyrolysis is conducted under an inert atmosphere at 300–600 °C, generating bio-oil, biochar, and syngas.

Recently, extensive research has been carried out to produce bio-oil and biochar from biomass through pyrolysis, showing that biofuels can be generated from first- and second-generation biomass, such as palm,[17] rice straw,[18] corn stover,[19] and sugarcane bagasse.[20] Yet, the massive use of first-generation biofuel feedstock may lead to competition between food and fuel, consequently increasing food prices.[21] Additionally, even though second-generation biomass does not compete with food, fresh water, fertilizer, and arable land are still required to produce biomass. To address this issue, third-generation biomass, such as macroalgae, have prospects to be used as feedstock for biofuels production. In fact, macroalgae have several advantages, including a faster growth rate, higher biomass yield, and shorter harvesting cycles than terrestrial plants.[1] Moreover, macroalgae are able to grow in seawater, freshwater, and wastewater.[22]

Among several species of macroalgae, the brown macroalgae *Sargassum* sp. is considered one of the most promising feedstocks for biofuels generation since it contains significant biomass resources and is globally abundant.[23] *Sargassum* typically contains a significant amount of carbohydrate (40–66% dry weight), followed by proteins (10–13%) and lipids (0.8–1.6%).[24] However, this biomass possesses a problem due to its unusual bloom and eutrophication in tropical seashores.[25] It has been reported that *Sargassum* can release large amounts of toxic gases, such as ammonia and hydrogen sulphide, raising human health concerns.[26] Furthermore, *Sargassum* decomposition results in the mortality of marine biota, including neritic fish and crustacea.[27] In this sense, valorizing *Sargassum* sp. as a third-generation biomass can offer a promising solution to solve the drawbacks of utilizing first- and second-generation biomass while overcoming marine pollution problems at the same.

In the context of the pyrolysis process, few studies regarding bio-oil production from *Sargassum* sp. have been reported.[28–30] Biswas *et al.*[28] found that the yield of a liquid product as high as 43.4% could be achieved at 450 °C. Furthermore, Cao *et al.*[29] reported that ZSM-5 could remarkably suppress the contents of N-containing and organic acid compounds, thus improving the algal bio-oil quality. Recently, Li *et al.*[30] performed the fast-pyrolysis of *Sargassum horneri* at 700–900 °C. Their results showed that the most prominent content in the liquid products of *S. horneri* pyrolysis was the N-containing compounds (up to 38.5%), which was a significant contrast with the liquid products from the pyrolysis of terrestrial plants.

Nevertheless, most of the previous studies only focused on the characteristics of bio-oil. A comprehensive study not only focusing on bio-oil but also biochar is thus necessary since biochar has great potential as a carbon material for energy storage, catalysis, wastewater treatment, supercapacitors, and microbial fuel cell electrodes.[31] Hence, the novelty of this study is emphasized as follows: (1) performing a comprehensive study for bio-oil and biochar production from *Sargassum* sp., including their characteristics that have not been reported previously and (2) providing the detailed reaction pathway for the conversion of *Sargassum* sp. into high-value compounds identified in bio-oil. This study thoroughly investigated the slow pyrolysis of *Sargassum* sp. for bio-oil and biochar production. More specifically, the objectives of this study were: (1) to examine the temperature effect on the product distribution of *Sargassum* sp.'s pyrolysis, (2) to investigate the effect of temperature on the chemical composition identified in bio-oil from the slow pyrolysis of *Sargassum* sp., (3) to study the characteristics of biochar, and (4) to determine the reaction kinetics of the slow pyrolysis of *Sargassum* sp.

Experimental

Feedstock preparation and analysis

The feedstocks of *Sargassum* sp. were collected from Ekas beach, Lombok Island, Indonesia. The samples were cleaned from sand/debris using tap water and deionized water. Afterwards, the cleaned samples were dried in an oven at 105 °C for 24 h. The dried macroalgae were subsequently ground and sieved to achieve a particle size of 0.25 mm.

Proximate analysis of the sample was determined using a thermogravimetric analyzer TGA 4000 (PerkinElmer, United States) following ASTM E1131-08. The mass loss determined the moisture content of the feedstock after the sample was heated at 110 °C using N_2 as a carrier gas. Meanwhile, the mass loss determined the volatile matter after the sample was heated to 900 °C. Afterwards, the N_2 was switched with air. The final amount of the sample remaining after being kept isothermally at 900 °C for 45 min was recorded as the ash content. The fixed carbon (FC) value was determined using the following formula:

$$\text{FC (wt\%)} = 100 - (\text{volatile matter wt\%} + \text{moisture wt\%} + \text{ash wt\%}).$$

Higher heating values (HHV) of feedstock were calculated using a bomb-calorimeter (Parr 6200 Isoperibol) according to ASTM D 5865-04. Furthermore, ultimate analysis of the carbon (C), hydrogen (H), and nitrogen (N) was determined using a CHN628 analyzer (Leco). Meanwhile, sulfur (S) analysis was carried out using a CHN632 analyzer (Leco). The oxygen (O) content was calculated using the formula as follows, O (%) = 100 – (%C + %H + %N + %S). All the analyses were conducted at least three times to obtain the reproducible data. Furthermore, the chemical constituents of the dried *Sargassum* sp. were

analyzed by PT. Saraswanti Indo Genetech (SIG)-Bogor, a laboratory service in Indonesia accredited to ISO/IEC 17025. The chemical constituent, proximate, and ultimate analyses of *Sargassum* sp. are summarized in Table S1.†

Pyrolysis of *Sargassum* sp.

The macroalgae *Sargassum* sp. was pyrolyzed in a batch reactor made of stainless steel (Fig. 1). The apparatus consisted of an electric furnace, thermocouple, a condenser, and a temperature controller. The thermocouple was installed to measure the actual temperature inside the reactor. This reactor allowed a maximum operating temperature up to 1000 °C to be regulated using a proportional integral derivative (PID) temperature controller. Briefly, 50 g of dried sample was placed in the reactor and purged with N_2 three times at a flow rate of 100 mL min^{-1} to ensure an oxygen-free atmosphere. The reactor was then heated at a heating rate of 30 °C min^{-1} from ambient temperature to the final temperature (400 °C, 500 °C, and 600 °C). The reactor was maintained at the final temperature for 10, 30, and 50 min. The vapour-phase products produced during the pyrolysis were condensed and collected in a liquid sampling port. The biochar was weighed *via* gravimetry and stored in a ziplock plastic bag for further analysis. All the experiments were conducted in duplicate to ensure reproducibility. The following equations were employed for the calculation of the yields of the products.

$$\text{Bio-oil yield } (\%) = \frac{\text{mass of bio-oil (g)}}{\text{intial mass of feedstock (g)}} \times 100 \quad (1)$$

$$\text{Biochar yield } (\%) = \frac{\text{mass of bio-char (g)}}{\text{intial mass of feedstock (g)}} \times 100 \quad (2)$$

$$\text{Gas yield } (\%) = 100 + (Y_{\text{bio-oil}} + Y_{\text{bio-char}}) \quad (3)$$

Characterization of the bio-oil and biochar

A gas chromatography/mass spectrometry (GC/MS-QP2010 SE–Shimadzu, Japan) system equipped with an Rtx®-5MS capillary column was used to characterize the bio-oil. The details of the bio-oil analysis using GC/MS have been reported in our previous studies.[32,33] Determination of the compounds in the bio-oil was conducted by comparing with the recorded mass spectra provided in the NIST2008 c2.0/Xcalibur data library.

Biochars obtained from the pyrolysis of *Sargassum* sp. were characterized by elemental (C, H, N, S) analysis, Fourier transform infrared spectroscopy (FTIR), scanning electron microscopy (SEM), and Brunauer–Emmett–Teller (BET) porosimetry. The biochar products' elemental composition (C, H, N, S, O) was determined with the same methods used for the feedstock. FTIR analysis was conducted using an infrared spectrometer Spectrum Two Universal ATR–FT-IR (PerkinElmer, United States) to evaluate the appearance of functional groups in the biochar. FTIR analysis was conducted in the 400–4000 cm^{-1} wavelength. The biochar morphology was also examined by SEM (Hitachi, SU 3500), operated using an electron acceleration of 20 kV. The images were captured at magnifications of 1000 and 2500×. The surface area, total pore volume, and mean pore diameter of the macroalgal biochar were characterized using a BET surface area and pore size analyzer with nitrogen adsorption at 77 K (Quantachrome Nova 4200e).

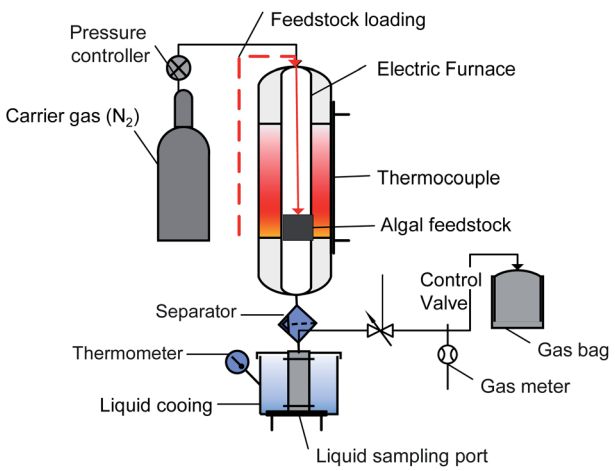

Fig. 1 Schematic diagram of the experimental apparatus.

Results and discussion

Effect of temperature on the product distribution

To investigate the temperature effect on the product distribution during the pyrolysis of *Sargassum* sp. in more detail, the pyrolysis was performed in the temperature range of 400–600 °C. It was observed that the biochar yield remarkably decreased with the increase in pyrolysis temperature from 400 °C to 600 °C (Fig. 2). This could be explained as due to the more significant primary decomposition of macroalgae biomass at higher temperatures. It is worth noting that the yield of bio-oil increased as the temperature increased from 400 °C to 500 °C, but the bio-oil yield decreased once the temperature increased further to 600 °C. The increase in bio-oil yield as the pyrolysis temperature increased from 400 °C to 500 °C could be attributed to an increase in the primary decomposition reactions of the algal biomass, such as from dehydration and thermal cracking. Meanwhile, the decrease in bio-oil yield as the pyrolysis temperature increased further to 600 °C was due to the further cracking of the products at a temperature above 500 °C, generating non-condensable gases, such as CH_4, CO, and CO_2, as reported in the previous study.[34,35] This was supported by the fact that the gas yield significantly increased with increasing the temperature from 400 °C to 600 °C. The enhancement of the gas yield might also be due to the high presence of alkali and alkaline earth metal species in the *Sargassum* sp. biomass, as indicated by the EDX analysis results (Fig. 3). The presence of these metals, such as potassium and calcium, enhanced the carbonaceous materials degradation, tar decomposition, and char reforming during pyrolysis and gasification to the gas product.[36]

At the lowest temperature of 400 °C, the bio-oil yields were relatively low. At this temperature, the bio-oil yield was merely 11.05% after a retention time of 10 min, reflecting the

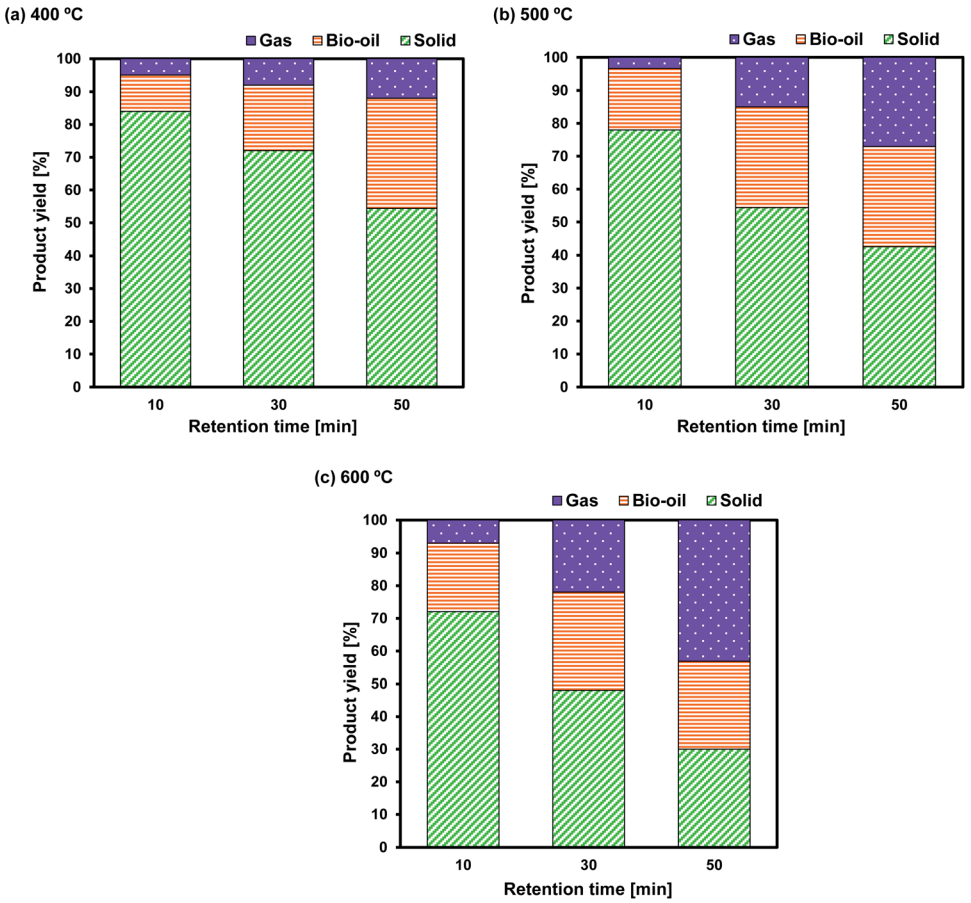

Fig. 2 Effect of temperature and retention time on the product distributions of *Sargasssum* sp. pyrolysis at (a) 400 °C; (b) 500 °C, and (c) 600 °C.

incomplete pyrolysis of *Sargassum* sp. The bio-oil yields increased to around 20.57% and 28.28% when the retention times were prolonged to 30 and 50 min, respectively, due to the significant occurrence of thermal cracking and dehydration reactions. As a result, these increased the liquid product yield. Additionally, the biochar yields significantly decreased with the retention time, demonstrating the evident decomposition of the algal biomass owing to the cracking of heavy hydrocarbons at the longer retention time. This finding was supported by the previous work of Choi *et al.*,[37] who observed that prolonging the holding time during the pyrolysis of *Saccharina japonica* could increase the bio-oil yield, but it decreased the biochar yield.

At 500 °C, the conversion of algal biomass to bio-oil was higher than that at 400 °C. Bio-oil yields of approximately

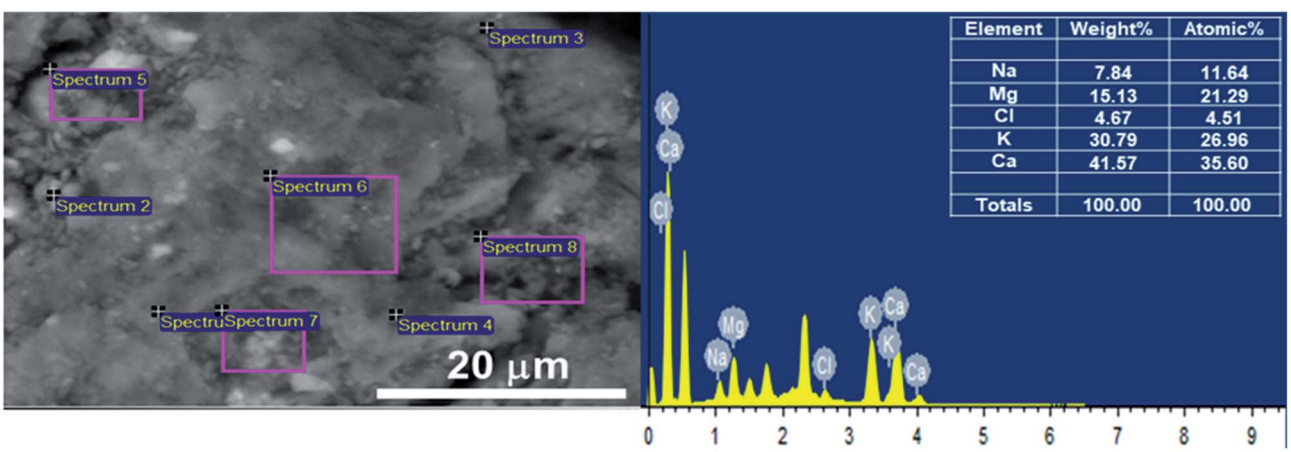

Fig. 3 Scanning electron microscopy - energy dispersive X-ray (SEM-EDX) analysis of the dried biomass of *Sargassum* sp.

18.46%, 29.86%, and 30.42% were obtained after 10, 30, and 50 min retention times, respectively. On the other hand, at a higher temperature of 600 °C, the longer retention time from 30 to 50 min did not significantly increase the bio-oil.

Overall, the increase in temperature from 400 °C to 600 °C accelerated the decrease in biochar yield and increase in gas products due to the further degradation of the biochar and secondary reactions of the volatile vapours. The results of this finding follow the previous studies.[35,37] Choi *et al.*[37] investigated the effect of temperature on the product distribution of *Saccharina japonica* pyrolysis in the temperature range of 430–530 °C. They observed that the biochar yield chiefly declined from 34.50 to 25.5 wt% when the temperature was increased from 430 °C to 530 °C. Meanwhile, the yield of gas steadily rose from 20.30 to 27.2 wt%. They also noticed that the pyrolysis temperature and heat transfer affected the product yield distribution. In another study by Aboulkas *et al.*,[35] the biochar yield from the pyrolysis of algal waste was found to significantly decrease from 52.09 to 40.36 wt% with the increase in temperature from 400 °C to 600 °C. The researchers in that study presumed that the decline in biochar yield might be due to either the more considerable decomposition of feedstock or the further thermal cracking of the biochar.

Characteristics of bio-oil

GC/MS analysis was conducted to determine the composition of bio-oil, in which the peak area percentage of the detected compounds is related to the response factor. The typical GC/MS spectra of *Sargassum*'s bio-oil is presented in Fig. S1.† As observed, the bio-oil product from the pyrolysis of *Sargassum* sp. exhibited a diverse mixture of compounds. It is worth noting that the bio-oil products derived from the slow pyrolysis of *Sargassum* sp. were primarily composed of aliphatic hydrocarbon, organic acids, amide, *N*-aromatic compounds, phenolics, and ketones.

To investigate its variability within the pyrolysis temperature, the peak area percentage of some compounds was used for comparison purposes. Only the main compounds with an area percentage higher than 0.5% were considered in this study. The results for the compounds identified in *Sargassum* sp. bio-oil at different temperatures are presented in Table S2.† At 400 °C, the three most abundant compounds observed from GC/MS were propionic acid (20.28%), acetic acid (11.26%), and 5-hydroxymethylfurfural/5-HMF (11.01). The formation of propionic and acetic acids has been linked to the thermal decomposition of lipids.[34] Meanwhile, 5-HMF formation is derived from the decomposition of cellulose.[38] The formation of propionic acid decreased while the acetic acid content steadily increased when the temperature was increased from 400 °C to 500 °C. This could be due to the decomposition of lipids, or long-chain carboxylic acid-generating short-chain carboxylic acid, which was enhanced with the rise in the pyrolysis temperature. It is worth noting that the formation of 5-HMF increased from 11.01% to 13.94% with increasing the temperature from 400 °C to 500 °C. This result could indicate that cellulose degradation to 5-HMF through the dehydration reaction is favourable at a temperature above 400 °C.[39] At the highest temperature of 600 °C, besides organic acids, a considerable amount of phenol was also observed. The formation of phenol might be derived from the interaction of the aromatic compound with steam/moisture during the pyrolysis of biomass.[38]

Based on the composition observed at different temperatures as shown in Table S2,† the chemical composition in *Sargassum* sp. bio-oil was as follows: carboxylic acids, furan derivatives, aliphatic hydrocarbons, *N*-aromatic compounds, phenolics, amines/amides, and ketones (Fig. 4). The major compounds were carboxylic acid with a 25–35 area%. The formation of short-chain carboxylic acids has been linked to the cracking of lipids. The result of this study is in line with the previous finding of Iaccarino *et al.*,[34] who observed that carboxylic acids were predominantly found in bio-oil from the pyrolysis of *Salicornia bigelovii*. It should be noted that the selectivity trend of carboxylic acids in the bio-oil decreased with the increase in the pyrolysis temperature, as follows: 35.01% (400 °C) > 31.68% (500 °C) > 25.07% (600 °C). This trend may be due to thermal cracking and the decarboxylation of organic acids generating short-chain aliphatic hydrocarbons with the increase in pyrolysis reaction. In fact, the trend of aliphatic hydrocarbons increased with the increase in pyrolysis temperature.

It is worth noting that fatty acid derivatives, such as *n*-hexadecanoic acid and 9,12-octadecadienoic acid, were also observed in small amounts during the pyrolysis of *Sargassum* sp. at 400 °C. The finding of this study follows the previous finding of Hong *et al.*,[40] who reported that macroalgae pyrolysis could generate *n*-hexadecanoic acid in small quantities. However, these compounds could not be observed at a temperature above 500 °C. As the temperature increased, *n*-hexadecanoic acid and 9,12-octadecadienoic acid were thermally decomposed into short-chain organic acids or aliphatic hydrocarbons. Fig. 5 shows the plausible reaction pathways from the slow pyrolysis of *Sargassum* sp.

Bio-oil derived from the pyrolysis of *Sargassum* sp. resulted in high amounts of furan derivatives, such as furfuryl alcohol and 5-HMF. Furan derivatives are generally obtained in the

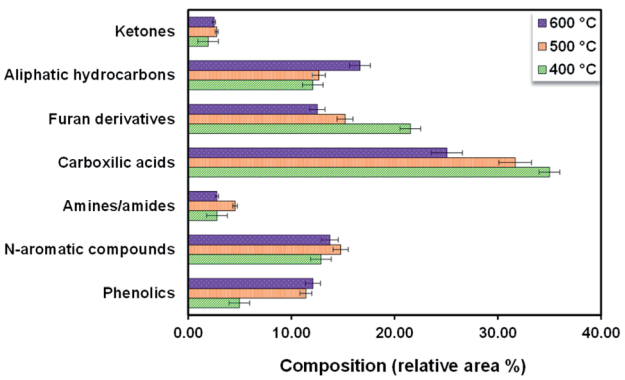

Fig. 4 Compounds observed in bio-oil from the pyrolysis of *Sargassum* sp. at varied temperatures.

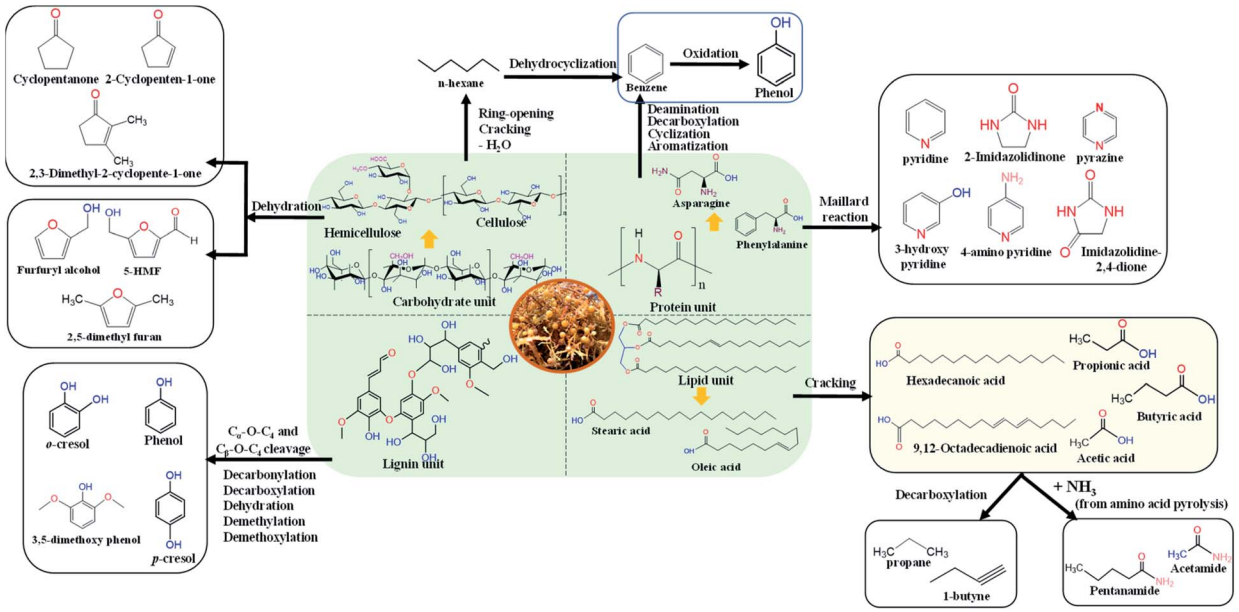

Fig. 5 Plausible reaction pathways from slow-pyrolysis of the *Sargassum* sp.

pyrolysis of glucose-based carbohydrates and seaweed polysaccharides.[39,41] Zhou *et al.*[42] reported that furan derivates might be derived from several steps of dehydration and ring-opening reactions of xylose. Another possibility for furan generation is *via* a concerted electrocyclic reaction followed by multiple steps of dehydration and cyclization. In this study, it was noticed that the selectivity of furan derivatives in the bio-oil decreased with the increase in temperature following the trend: 21.53% (400 °C) > 15.21% (500 °C) > 12.51% (600 °C). This trend could be attributed to the ring-opening and cracking of furan derivates to generate the hydrocarbons being enhanced with the increase in the temperature.

It is worth mentioning that the pyrolysis of *Sargassum* sp. displayed a higher amount of *N*-aromatic compounds (12.86–14.78%) than that of other terrestrial lignocellulosic biomasses.[43–45] This could be due to the macroalgae having a higher protein content than terrestrial lignocellulosic biomass.[1] The formation of *N*-aromatic compounds is commonly derived from protein decomposition into amino acids at high pyrolysis temperatures, followed by the cyclization and aromatization reactions of amino acids. Another possibility is the reaction of the amino acids and carbohydrates through the Maillard reaction, which can further decompose to generate *N*-aromatic compounds.[46] The main component of *N*-aromatic compounds observed in this study was heterocyclic derivatives, such as pyrazine, pyridine, 3-hydroxy pyridine, 2-imidazolidinone, and 4-aminopyridine. The finding of this study follows the previous research by Iaccarino *et al.*,[34] who reported that amino acids could undergo decarboxylation, cyclization, and dehydration to generate the N-heterocyclic derivatives during the pyrolysis of *Salicornia bigelovii*.

Phenolic compounds in the bio-oil from *Sargassum* sp. pyrolysis were present in a few amounts. Selectivities of phenolic compounds of 4.96%, 11.41%, and 12.10% were observed at 400 °C, 500 °C, and 600 °C, respectively. This contrasts with the pyrolysis of terrestrial lignocellulosic biomass, where phenolic compounds are produced in abundance (28.1–65.56%).[47,48] This difference could be attributed to the lignin content in macroalgae being lower than that in terrestrial plant biomass. The formation of phenolic derivatives also has been linked to the thermal decomposition of proteins, especially protein-containing phenylalanine.[35] The phenolic compounds may also be derived from the interaction of moisture with aromatic compounds, as reported by Gautam *et al.*[38] and some phytochemical metabolites in *Sargassum* sp. It should be noted that brown macroalgae, like *Sargassum* sp., are rich in phenolic secondary metabolites, such as tannins, flavonoids, and phenols, which function as their chemical defence towards UV sunlight exposure.[49]

The major hydrocarbons observed in the bio-oil from *Sargassum* sp were propane and 1-butyne. These aliphatic hydrocarbons were mainly generated from organic acids' cracking and decarboxylation reactions. The selectivity of aliphatic hydrocarbons in the bio-oil increased with the temperature following the trend: 12.08% (400 °C) < 12.65% (500 °C) < 16.65% (600 °C). The aliphatic hydrocarbons could be generated from the ring-opening, cracking, and dehydration of cellulose, as reported by Iaccarino *et al.*[34] Macroalga *Sargassum* sp. also produces a trace amount of amine/amide compounds, such as butylamine, acetamide, and pentanamide. The formation of amine derivatives has been primarily linked to the decarboxylation and decomposition of amino acids. Meanwhile, the amide compounds were plausibly derived from the reaction of organic acids and the ammonium produced from the decomposition of amino acids during pyrolysis. Moreover, the main ketones found in the *Sargassum* sp. bio-oil were cyclopentanone, 2-cyclopentene-1-one, and 2,3-dimethyl-2-cyclopentene-1-one. The formation of ketones mainly occurs

as typical pyrolysis products of cellulose and hemicellulose decomposition, which have been reported in the literature.[50,51]

Characteristics of biochar

Biochar obtained was analyzed in terms of elemental composition, FTIR, and SEM to better understand the pyrolysis behaviour of *Sargassum* sp.

Elemental composition

Table 1 displays the calorific value and ultimate analysis of *Sargassum* sp. biochar obtained at 400 °C, 500 °C, and 600 °C. The value of the feedstock is presented here for comparison purposes. The biochars obtained from the pyrolysis of *Sargassum* sp. had a high carbon content (51.28–54.01%), low hydrogen content (2.89–3.05%), and moderate oxygen content (39.48–41.82%). As presented in Table 1, the biochar had a higher C content than the macroalgal feedstock. In addition, the C content in the biochar increased with temperature. Meanwhile, the biochar's O and H contents were lower than the feedstock, which may be due to the dehydration, decarboxylation, and decarbonylation reactions during the pyrolysis. In contrast, the hydrogen value in the biochar relatively decreased with temperature following the trend: 3.05% (400 °C) > 2.99% (500 °C) > 2.89% (600 °C). Furthermore, the trend for the oxygen content of the biochar also declined with temperature.

The reduction of hydrogen and oxygen might be because the dehydration and deoxygenation reactions were enhanced with the increase in temperature. The low hydrogen content of biochar was also possibly due to the aromatization and formation of hydrogen gas (H_2) as a result of the generation of the low-molecular-weight hydrocarbons (CH_4, C_2H_6, or C_2H_4).[35] It should be noted that the nitrogen content of biochar derived from macroalgal pyrolysis decreased with the increasing pyrolysis temperature. This may be because nitrogen is released in the gas phase as the pyrolysis temperature increases. It is intriguing to mention that the HHV of biochar from the macroalgal pyrolysis was in the range of 23.12–25.89 MJ kg^{-1}, which is relatively higher than those of the low-ranked coals (12–25 MJ kg^{-1}, although the typical value is ~15 MJ kg^{-1}).[53] The high calorific values and carbon content indicate macroalgal biochar has potential to be utilized as a solid renewable fuel. Furthermore, the ultimate analysis of low-rank coal-lignite is also presented in Table 1 for comparison purposes. The ultimate analysis of macroalgal biochar is comparable with the low-rank coal-lignite. The sulfur content of low-rank coal-lignite varies from 0.3% to 6.0%, depending on the location and geological processes.[52] Solid fuels with a low sulfur content are more environmentally friendly since the oxidation product of sulfur can cause corrosion and pollution.

The critical parameters to assess the characteristics of biomass for energy application besides the HHV are the atomic ratios of O/C and H/C. According to Zhao *et al.*,[54] C–O and C–H bonds contain lower chemical energies than C–C; hence, biomass having lesser atomic ratios of O/C and H/C mainly contains a higher energy content. The evolution of O/C and H/C atomic ratios from the pyrolysis of *Sargassum* sp. by the Van Krevelen diagram is presented in Fig. 6. It should be noted that the O/C and H/C atomic ratios of biochar were lower than that of the feedstock, confirming that dehydration and decarboxylation reactions occurred throughout the pyrolysis. The H/C atomic ratio of macroalgal feedstock significantly decreased from 1.66 to 0.71, 0.75, and 0.79 for the pyrolysis temperatures of 400 °C, 500 °C, and 600 °C, respectively. Likewise, the O/C atomic ratio of macroalgal feedstock also decreased from 0.82 to 0.62, 0.58, and 0.54 for the pyrolysis temperatures of 400 °C, 500 °C, and 600 °C, respectively. Zhou *et al.*[55] presumed that the decrease in the bond energies of C–H and C–O and the increase in bond energy of C–C could enhance the energy content of biochar. In fact, the calorific values of biochar obtained from the *Sargassum* sp. pyrolysis were higher than those of the feedstock. Moreover, Gasco *et al.*[56] pointed out that low O/C and H/C atomic ratios indicated a high carbon stability and high aromatic derivatives.

FTIR characterization

FTIR analysis was used to characterize the functional groups in the biochar obtained from the *Sargassum* sp. pyrolysis. The FTIR spectra of biochar at different temperatures are shown in Fig. 7. The details of the typical band assignment of biochar at different temperatures are presented in Table S3.† It is intriguing to note that the peak at 3600–3100 cm^{-1} (O–H stretching vibration) was absent in the FTIR spectra, confirming the dehydration reaction during the pyrolysis. Small bands of aliphatic C–H stretching at 2815–2860 cm^{-1} were observed. However, this band disappeared when the temperature was increased from 400 °C to 600 °C. This may be due to C–H alkyl groups' cracking at high pyrolysis temperatures. The band at 1625 cm^{-1} was assigned to the aromatic C=C ring stretching. Meanwhile, the medium peak at 1422 cm^{-1} indicated the aliphatic C–H bending. The strong peaks 1095–1098 cm^{-1} were correlated to stretching vibrations from the aromatic C–H group. These peaks indicated that the biochar contained aromatic compounds. Moreover, a few peaks at 873 cm^{-1} were observed, which were closely linked to the existence of polycyclic aromatic hydrocarbons (PAHs), which could be generated

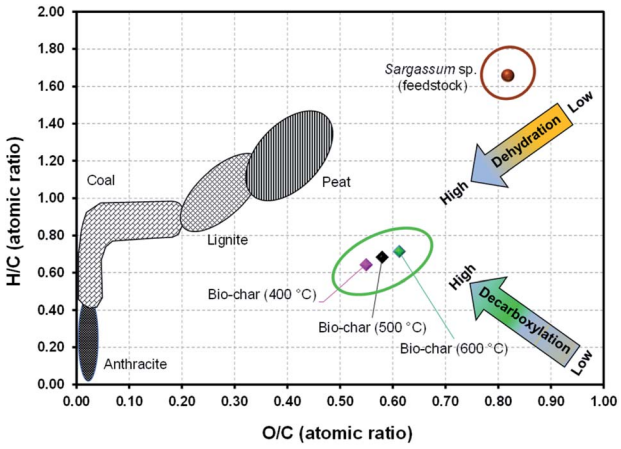

Fig. 6 Van Krevelen diagram of the biochar derived from *Sargassum* sp. pyrolysis.

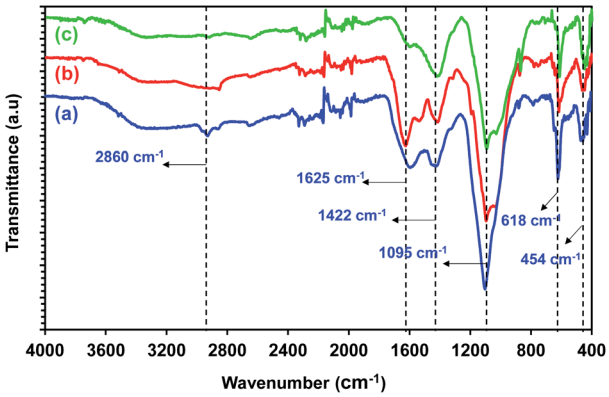

Fig. 7 FTIR spectra of the biochar from *Sargassum* sp. pyrolysis at (a) 400 °C, (b) 500 °C, and (c) 600 °C.

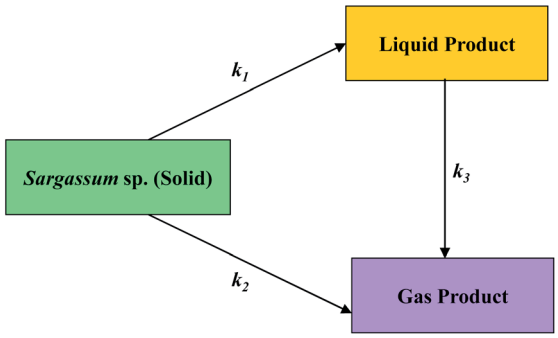

Fig. 9 Reaction pathway of macroalgae decomposition during pyrolysis.

throughout the pyrolysis of typical biomass.[34] The trend in the FTIR spectra observed in this study followed the trend observed in a previous study by Aboulkas *et al.*[35] They reported that the biochar derived from algal waste pyrolysis displayed peaks for C–H stretching (2852–2960 cm^{-1}), C=C stretching (1656 cm^{-1}), and heteroatom functional groups (1730–1150 cm^{-1}).

Overall, the FTIR spectra of biochar from the pyrolysis of *Sargassum* sp. indicated the presence of aromatic compounds. This could be attributed to the fact that biochar comprised polycyclic aromatic compounds.[35] The results from the FTIR spectra were in good agreement with the ultimate analysis, which confirmed the high carbon content in the biochar.

Scanning electron microscopy

SEM was used to investigate the surface morphology of the macroalgal feedstock and its biochar. Fig. 8 depicts a comparison of the SEM photographs for the feedstock and its biochar derived from the *Sargassum* sp. pyrolysis at different pyrolysis temperatures. It was clearly shown that the macroalgal feedstock displayed different characteristics to its biochar in terms of its morphologies. Interestingly, the surface morphology of the biochar had a higher porosity than the macroalgal feedstock. This may be because the high pyrolysis temperature could deform the surface of *Sargassum* sp., leading to a higher porous structure of the biochar. The morphological structures of several kinds of biomass-derived biochars were comprehensively reviewed by Leng *et al.*[57] However, macroalgal biochar was

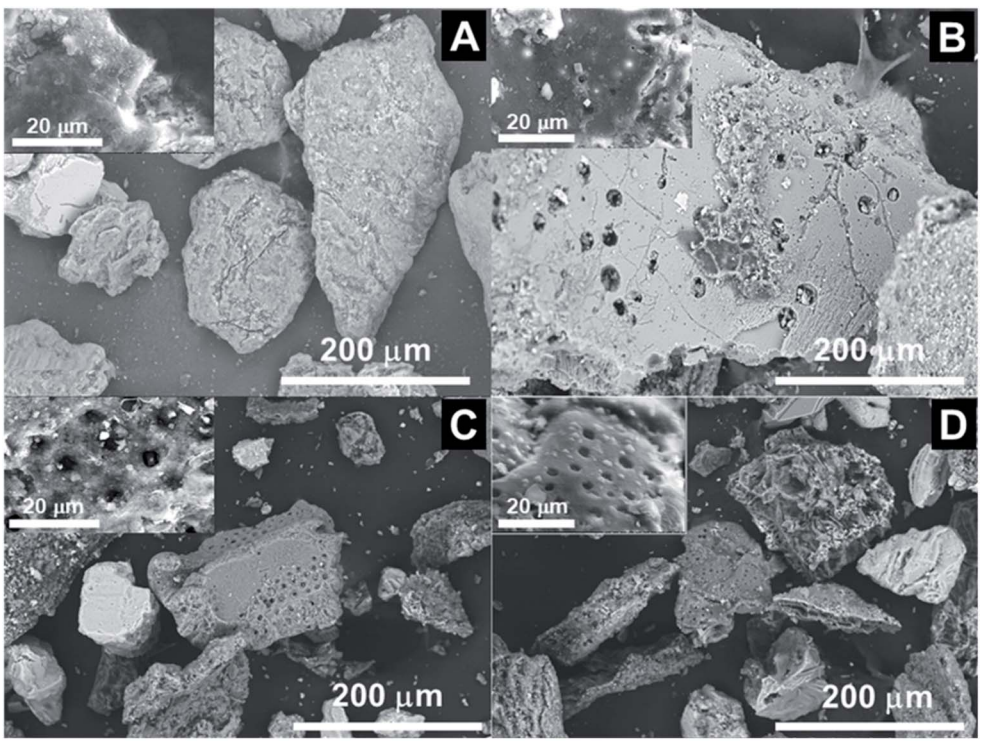

Fig. 8 SEM images of (A) untreated *Sargassum* sp.; (B) biochar at 400 °C; (C) biochar at 500 °C; and (D) biochar at 600 °C.

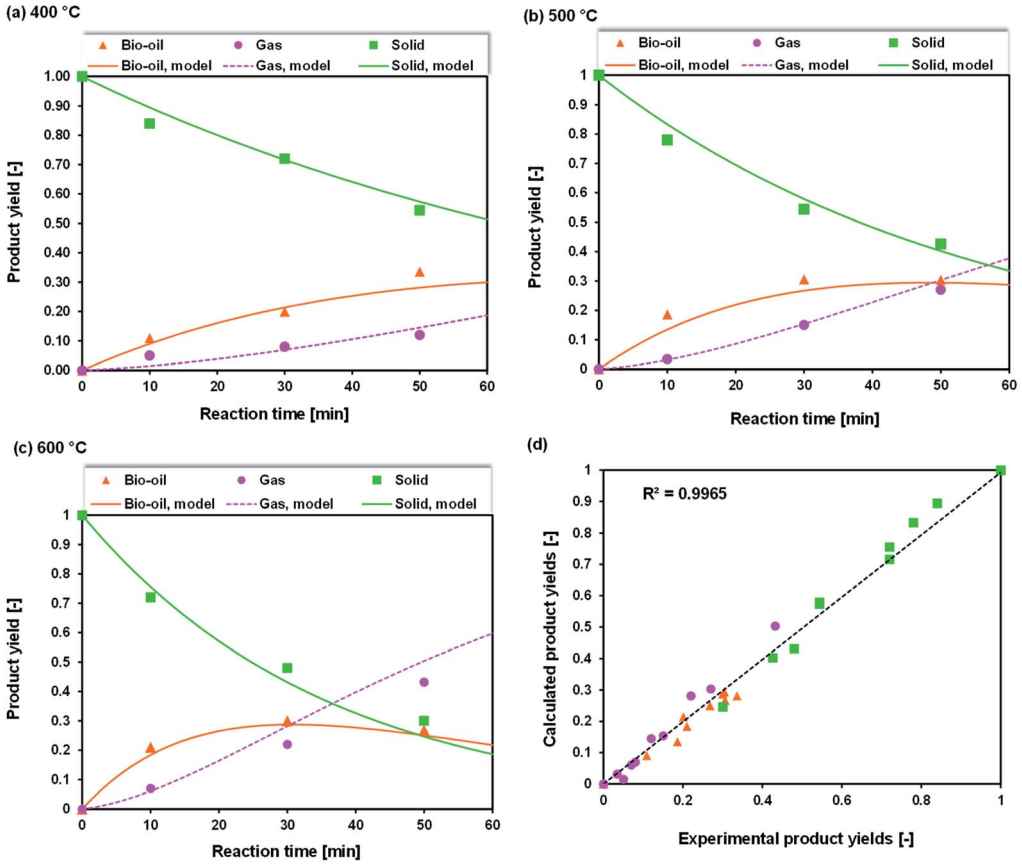

Fig. 10 Product distribution from experiments (symbol) and kinetic modelling (line) at (a) 400 °C, (b) 500 °C, (c) 600 °C and (d) parity plot.

not taken into account in that study. This might have been because the investigation of biochar from macroalgae is still rarely performed. They summarized that lignocellulosic biomass (sugar cane and Durian wood sawdust)-based biochars are more porous than those derived from microalgae *C. vulgaris* and sewage sludge. The morphological structure of macroalgae *Sargassum*-derived biochar obtained from this study was comparable with that of *C. vulgaris*. However, the morphological structure of macroalgal biochar was more porous than that of the microalgal biochar. This could be attributed to the macroalgae having a higher carbohydrate content than microalgae.[1] The details of Sargassum sp.'s pore size and its biochar are presented in Fig. S2.† Moreover, the BET surface area, total pore volume, and mean pore diameter of the macroalgal biochar are summarized in Table S4.† The BET surface area of *Sargassum* sp. biochar was in the range 4.28–5.68 $m^2 g^{-1}$. In addition, the mean pore diameter of the macroalgal biochar was in the range 10.83–12.20 nm, confirming that the biochar derived from *Sargassum* sp. could be classified as a mesoporous material. The BET surface area of the macroalgal biochar was significantly lower than that of biochar from pigeon pea stalk (16.90 to 261.78 $m^2 g^{-1}$).[58] This could be attributed to the lower lignin content in macroalgal biomass than in terrestrial plant biomass. Having said that, the BET surface area from this study was comparable with the previous work of Iaccarino *et al.*,[34] who observed that the surface area of biochar from *Salicornia bigelovii* was in the range 1.30–2.35 $m^2 g^{-1}$. Furthermore, it could be confirmed from this study that an increase in the pyrolysis temperature led to an increase in the BET surface area and total pore volume, which could be because more volatile matter and pore-blocking substances from the biomass matrix were released, resulting in more

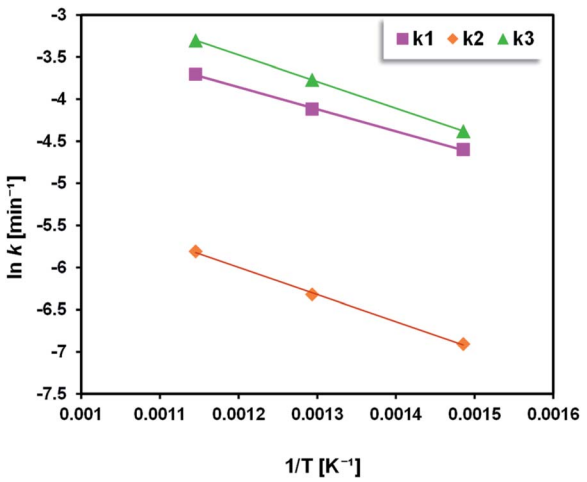

Fig. 11 Arrhenius plot of *Sargassum* sp. pyrolysis (exp. conditions: 400–600 °C).

Table 1 Elemental analysis of biochar from the pyrolysis of *Sargassum* sp.

	Ultimate analysis (wt%, dry ash-free)					
Sample	% C	% H	% N	% S	% O	HHV (MJ kg^{-1})
Feedstock	42.40 ± 0.38	5.86 ± 0.03	2.72 ± 0.01	2.78 ± 0.05	46.24 ± 0.30	14.46 ± 0.08
Biochar (400 °C)	51.28 ± 0.06	3.05 ± 0.06	1.38 ± 0.02	2.48 ± 0.06	41.82 ± 0.04	23.12 ± 0.06
Biochar (500 °C)	52.58 ± 0.06	2.99 ± 0.04	1.32 ± 0.01	2.45 ± 0.03	40.65 ± 0.04	24.12 ± 0.09
Biochar (600 °C)	54.01 ± 1.12	2.89 ± 0.07	1.24 ± 0.03	2.38 ± 0.04	39.48 ± 0.90	25.89 ± 0.10
Low-rank coal-lignite[52]	58.78	4.9–7.0	0.6–2.4	0.3–6.0	12–30	12.00–25.0053

Table 2 Activation energies (E_a) obtained for pyrolysis of *Sargassum* sp. (experimental conditions: 400–600 °C)

Kinetic parameter	Reaction direction	Activation energy, E_a [kJ mol^{-1}]	Pre-exponential factor, A [s^{-1}]
k_1	Solid → liquid	21.83	8.22×10^{-3}
k_2	Solid → gas	26.77	1.97×10^{-3}
k_3	Liquid → gas	26.31	2.30×10^{-2}

pores in the biochar. After all, this result provides insights for future research in developing renewable porous carbon-based materials from macroalgae *Sargassum* sp. for the applications as adsorbents and catalysts, and in wastewater treatment and energy storage.

Kinetic modelling of macroalgae pyrolysis

The kinetics of macroalgal pyrolysis were determined to quantify the effect of temperature on the product distribution. A kinetic model was determined based on the solid, liquid, and gas yields. The mechanism of decomposition of the macroalgae during pyrolysis is depicted in Fig. 9. The feedstock (solid) was immediately decomposed into a liquid (k_1). Meanwhile, some solid feedstocks were converted to the gaseous products (k_2). In either way, the liquid product was also changed to produce gas (k_3).

Based on the reaction pathways above, the rate of change in the product yield could be manifested by the equations of the differential rate as follows:

$$\mathrm{d}Y\,(\text{solid})/\mathrm{d}t = (k_1 + k_2)\,Y\,(\text{solid}) \quad (4)$$

$$\mathrm{d}Y\,(\text{liquid})/\mathrm{d}t = (k_1 Y)\,(\text{solid}) - (k_3 Y)\,(\text{liquid}) \quad (5)$$

$$\mathrm{d}Y\,(\text{gas})/\mathrm{d}t = (k_2 Y)\,(\text{solid}) + (k_3 Y)\,(\text{liquid}) \quad (6)$$

where k represents reaction rate constant [s^{-1}], t represents reaction time [min], and $Y(X)$ represents the product yield [−].

Non-linear regression was employed to determine the reaction rate constants. In this study, the least-squares-error (LSE) method was employed. Fig. 10(a)–(c) show the comparisons of the experimental product yield and calculated values (lines). As shown in Fig. 10(d), a high r^2 (coefficient of determination) value was achieved, confirming that the model could reproduce the trends of most the product yields proportional to the different temperatures and reaction times.

The correlation of the temperature on the rate constants was determined by the Arrhenius equation (eqn (6)) to calculate the activation energy and pre-exponential factor.

$$k = A\mathrm{e}^{(-E_a/RT)} \quad (7)$$

where E_a is the activation energy [kJ mol^{-1}], T is the reaction temperature [K], R is the reaction rate constant of universal gas [8.314 J mol^{-1} K^{-1}], and A is the pre-exponential factor [min^{-1}].

Fig. 11 shows the Arrhenius plots for the pyrolysis of *Sargassum* sp. As expected, the straight line between the inverse temperatures ($1/T$) and the logarithm of the reaction rate constant (ln k) could be noticed, confirming that the distribution product of macroalgal pyrolysis obeyed the Arrhenius equation. The values for the activation energies and pre-exponential factors obtained for the pyrolysis of *Sargassum* sp. are presented in Table 2. Activation energies between 21.83 to 26.77 kJ mol^{-1} were obtained for *Sargassum* sp. pyrolysis. Pre-exponential factors of 8.22×10^{-3}, 1.97×10^{-3}, and 2.30×10^{-2} s^{-1} were obtained to convert solid to liquid, solid to gas, and liquid to gas products, respectively. Interestingly, the activation energy for the conversion of solid to gas was higher (26.77 kJ mol^{-1}) than that for solid to liquid (21.83 kJ mol^{-1}). This could be attributed to the fact that the energy needed to decompose solid into gas products is higher than for converting the solids to liquids.

Conclusions

The slow pyrolysis of *Sargassum* sp. was investigated comprehensively for bio-oil and biochar production. The bio-oil derived from *Sargassum* sp. pyrolysis primarily contained carboxylic acids (25.07–35.01%), furan derivatives (12.51–21.53%), aliphatic hydrocarbons (12.08–16.65%), and *N*-aromatic compounds (12.86–14.78%). The biochars' H/C and O/C atomic ratios were lower than those of the feedstock, confirming that dehydration and decarboxylation reactions occurred

throughout the pyrolysis. The heating values and carbon content of macroalgal biochar increased with temperature. The higher heating value (HHV) of biochar from the macroalgal pyrolysis was in the range of 23.12–25.89 MJ kg^{-1}, which was relatively higher than those of the low-ranked coals. Intriguingly, SEM analysis showed a higher porosity in the biochar surface compared to in the original feedstock, indicating that *Sargassum*'s-derived biochar has excellent potential as a renewable porous carbon-based material for application as an adsorbent and catalyst, or in wastewater treatment and energy storage. The BET surface area of *Sargassum* sp. biochar was in the range 4.28–5.68 $m^2 g^{-1}$. The kinetic model of *Sargassum* sp. pyrolysis was proposed, and it was found that the experimental data agreed well with the kinetic model. The activation energies were calculated to be between 21.83 and 26.77 kJ mol^{-1}. A significant overall finding from the pyrolysis of *Sargassum* sp. would be more beneficial if all the resulting products could be used appropriately. Hence, further investigations into integrating the downstream processes to further valorize *Sargassum* sp. for bioenergy and value-added need to be conducted in the future.

CRediT authorship contribution statement

Obie Farobie: conceptualization, methodology, writing-original draft, resources, formal analysis, project administration, funding acquisition. Apip Amrullah: methodology, investigation, resources, formal analysis. Asep Bayu: writing-review and editing, investigation, resources. Novi Syaftika: investigation, resources. Latifa A. Anis: investigation. Edy Hartulistiyoso: writing-review and editing, supervision.

Conflicts of interest

There are no conflicts to declare.

Acknowledgements

The authors are enormously grateful to IPB University through World-Class University-Program Riset Kerjasama Institusi (RKI) (9072/IT3.L1/PT.01.03/P/B/2021). The research funding from Indonesian Endowment Fund for Education (LPDP) and the Indonesian Science Fund (DIPI) through the RISPRO Kolaborasi Internasional (RISPRO-KI) Funding Program (Grant No. RISPRO/KI/B1/KOM/12/11684/1/2020) are also duly acknowledged. The APC was funded by Indonesian Endowment Fund for Education (LPDP) through RISPRO-KI Funding Program. We thank the National Research and Innovation Agency (BRIN), for providing the instrumental analysis of CHNS analyzer, FTIR, and SEM.

Notes and references

1 O. Farobie, Y. Matsumura, N. Syaftika, A. Amrullah, E. Hartulistiyoso, A. Bayu, N. R. Moheimani, S. Karnjanakom and G. Saefurahman, *Bioresour. Technol. Rep.*, 2021, **16**, 100844.
2 J. Q. Bond, A. A. Upadhye, H. Olcay, G. A. Tompsett, J. Jae, R. Xing, D. M. Alonso, D. Wang, T. Zhang, R. Kumar, A. Foster, S. M. Sen, C. T. Maravelias, R. Malina, S. R. H. Barrett, R. Lobo, C. E. Wyman, J. A. Dumesic and G. W. Huber, *Energy Environ. Sci.*, 2014, **7**, 1500–1523.
3 F. Abnisa and W. M. A. Wan Daud, *Energy Convers. Manage.*, 2014, **87**, 71–85.
4 M. A. Destek, S. A. Sarkodie and E. F. Asamoah, *Biomass Bioenergy*, 2021, **149**, 106076.
5 C. Y. Li, J. Y. Wu, Y. J. Dai and C. H. Wang, *Energy Convers. Manage.*, 2021, **243**, 114364.
6 X. Zhang, H. Lei, S. Chen and J. Wu, *Green Chem.*, 2016, **18**, 4145–4169.
7 V. Dhyani and T. Bhaskar, *Renewable Energy*, 2018, **129**, 695–716.
8 W. Yang, Z. Wang, J. Han, S. Song, Y. Zhang and W. Gong, *RSC Adv.*, 2019, **9**, 41962–41969.
9 N. Nkosi, E. Muzenda, J. Gorimbo and M. Belaid, *RSC Adv.*, 2021, **11**, 11844–11871.
10 O. Farobie, P. Changkiendee, S. Inoue, T. Inoue, Y. Kawai, T. Noguchi, H. Tanigawa and Y. Matsumura, *Ind. Eng. Chem. Res.*, 2017, **56**, 6401–6407.
11 T. Samanmulya, O. Farobie and Y. Matsumura, *J. Jpn. Pet. Inst.*, 2017, **60**, 34–40.
12 A. Horvat, D. S. Pandey, M. Kwapinska, B. B. Mello, A. Gómez-Barea, L. E. Fryda, L. P. L. M. Rabou, W. Kwapinski and J. J. Leahy, *RSC Adv.*, 2019, **9**, 13283–13296.
13 J. Chen and S. Li, *RSC Adv.*, 2020, **10**, 2160–2169.
14 S. Budsaereechai, A. J. Hunt and Y. Ngernyen, *RSC Adv.*, 2019, **9**, 5844–5857.
15 J. Wu, L. Wang, H. Ma and J. Zhou, *RSC Adv.*, 2021, **11**, 34795–34805.
16 R. P. Anex, A. Aden, F. K. Kazi, J. Fortman, R. M. Swanson, M. M. Wright, J. A. Satrio, R. C. Brown, D. E. Daugaard, A. Platon, G. Kothandaraman, D. D. Hsu and A. Dutta, *Fuel*, 2010, **89**, S29–S35.
17 L. M. Terry, C. Li, J. J. Chew, A. Aqsha, B. S. How, A. C. M. Loy, B. L. F. Chin, D. S. Khaerudini, N. Hameed, G. Guan and J. Sunarso, *Carbon Resour. Convers.*, 2021, **4**, 239–250.
18 A. K. Sakhiya, A. Anand, I. Aier, V. K. Vijay and P. Kaushal, *Bioresour. Technol. Rep.*, 2021, **15**, 100818.
19 E. Hu, Y. Tian, Y. Yang, C. Dai, M. Li, C. Li and S. Shao, *J. Anal. Appl. Pyrolysis*, 2022, **161**, 105398.
20 C. A. Okonkwo, M. C. Menkiti, I. A. Obiora-Okafo and O. N. Ezenwa, *Biomass Bioenergy*, 2021, **146**, 105996.
21 M. C. Rulli, D. Bellomi, A. Cazzoli, G. De Carolis and P. D'Odorico, *Sci. Rep.*, 2016, **6**, 1–10.
22 H. V. Ly, S. S. Kim, H. C. Woo, J. H. Choi, D. J. Suh and J. Kim, *Energy*, 2015, **93**, 1436–1446.
23 D. Davis, R. Simister, S. Campbell, M. Marston, S. Bose, S. J. McQueen-Mason, L. D. Gomez, W. A. Gallimore and T. Tonon, *Sci. Total Environ.*, 2021, **762**, 143134.
24 M. Farghali, A. P. Yuhendra, I. M. A. Mohamed, M. Iwasaki, S. Tangtaweewipat, I. Ihara, R. Sakai and K. Umetsu, *J. Environ. Chem. Eng.*, 2021, **9**, 106405.

25 S. Saldarriaga-Hernandez, E. F. Nájera-Martínez, M. A. Martínez-Prado and E. M. Melchor-Martínez, *Case Stud. Chem. Environ. Eng.*, 2020, **2**, 100032.
26 D. Resiere, R. Valentino, R. Nevière, R. Banydeen, P. Gueye, J. Florentin, A. Cabié, T. Lebrun, B. Mégarbane, G. Guerrier and H. Mehdaoui, *Lancet*, 2018, **392**, 2691.
27 R. E. Rodríguez-Martínez, A. E. Medina-Valmaseda, P. Blanchon, L. V. Monroy-Velázquez, A. Almazán-Becerril, B. Delgado-Pech, L. Vásquez-Yeomans, V. Francisco and M. C. García-Rivas, *Mar. Pollut. Bull.*, 2019, **146**, 201–205.
28 B. Biswas, R. Singh, B. B. Krishna, J. Kumar and T. Bhaskar, *Bioresour. Technol.*, 2017, **242**, 139–145.
29 B. Cao, Z. Xia, S. Wang, A. E. F. Abomohra, N. Cai, Y. Hu, C. Yuan, L. Qian, L. Liu, X. Liu, B. Li, Z. He and Q. Wang, *J. Anal. Appl. Pyrolysis*, 2018, **134**, 526–535.
30 J. Li, Y. Zhu, C. Wang, W. Wei, Z. Liu, Y. Tian, P. Zong, Y. Qiao and S. Qin, *Algal Res.*, 2020, **48**, 101888.
31 I. Ali and A. Bahadar, *Algal Res.*, 2017, **21**, 89–97.
32 A. Amrullah, O. Farobie and R. Widyanto, *Bioresour. Technol. Rep.*, 2021, **13**, 100642.
33 A. Amrullah, O. Farobie and G. P. Pramono, *Korean J. Chem. Eng.*, 2022, **39**, 389–397.
34 A. Iaccarino, R. Gautam and S. M. Sarathy, *Sustainable Energy Fuels*, 2021, **5**, 2234–2248.
35 A. Aboulkas, H. Hammani, M. El Achaby, E. Bilal, A. Barakat and K. El harfi, *Bioresour. Technol.*, 2017, **243**, 400–408.
36 M. Kaewpanha, G. Guan, X. Hao, Z. Wang, Y. Kasai, K. Kusakabe and A. Abudula, *Fuel Process. Technol.*, 2014, **120**, 106–112.
37 J. H. Choi, S. S. Kim, D. J. Suh, E. J. Jang, K. Il Min and H. C. Woo, *Korean J. Chem. Eng.*, 2016, **33**, 2691–2698.
38 R. Gautam, S. Shyam, B. R. Reddy, K. Govindaraju and R. Vinu, *Sustainable Energy Fuels*, 2019, **3**, 3009–3020.
39 S. Wang, Z. Xia, Q. Wang, Z. He and H. Li, *J. Anal. Appl. Pyrolysis*, 2017, **126**, 118–131.
40 Y. Hong, W. Chen, X. Luo, C. Pang, E. Lester and T. Wu, *Bioresour. Technol.*, 2017, **237**, 47–56.
41 R. Vinu and L. J. Broadbelt, *Energy Environ. Sci.*, 2012, **5**, 9808–9826.
42 X. Zhou, W. Li, R. Mabon and L. J. Broadbelt, *Energy Environ. Sci.*, 2018, **11**, 1240–1260.
43 H. Persson and W. Yang, *Fuel*, 2019, **252**, 200–209.
44 L. Zhang, Z. Yang, S. Li, X. Wang and R. Lin, *J. Anal. Appl. Pyrolysis*, 2020, **152**, 104966.
45 P. Zong, Y. Jiang, Y. Tian, J. Li, M. Yuan, Y. Ji, M. Chen, D. Li and Y. Qiao, *Energy Convers. Manage.*, 2020, **216**, 112777.
46 X. Wang, X. Tang and X. Yang, *Energy Convers. Manage.*, 2017, **140**, 203–210.
47 Y. Su, L. Liu, S. Zhang, D. Xu, H. Du, Y. Cheng, Z. Wang and Y. Xiong, *Bioresour. Technol.*, 2020, **295**, 122243.
48 Z. B. Zhang, Q. Lu, X. N. Ye, W. T. Li, B. Hu and C. Q. Dong, *Energy Convers. Manage.*, 2015, **106**, 1309–1317.
49 M. F. Nazarudin, N. H. Alias, S. Balakrishnan, W. N. I. Wan Hasnan, N. A. I. Noor Mazli, M. I. Ahmad, I. S. Md Yasin, A. Isha and M. Aliyu-Paiko, *Molecules*, 2021, **26**, 5216.
50 C. Zhao, E. Jiang and A. Chen, *J. Energy Inst.*, 2017, **90**, 902–913.
51 L. Reyes, L. Abdelouahed, C. Mohabeer, J. C. Buvat and B. Taouk, *Energy Convers. Manage.*, 2021, **244**, 114459.
52 H. Pawlak-Kruczek, *Properties of low rank coals and resulting challenges in their utilization*, Elsevier Ltd, 2017.
53 Z. Luo and W. Tao, *CFBC and BFBC of low-rank coals*, Elsevier Ltd, 2017.
54 P. Zhao, Y. Shen, S. Ge, Z. Chen and K. Yoshikawa, *Appl. Energy*, 2014, **131**, 345–367.
55 S. Zhou, H. Liang, L. Han, G. Huang and Z. Yang, *Waste Manag.*, 2019, **88**, 85–95.
56 G. Gascó, J. Paz-Ferreiro, M. L. Álvarez, A. Saa and A. Méndez, *Waste Manag.*, 2018, **79**, 395–403.
57 L. Leng, Q. Xiong, L. Yang, H. Li, Y. Zhou, W. Zhang, S. Jiang, H. Li and H. Huang, *Sci. Total Environ.*, 2021, **763**, 144204.
58 S. S. Sahoo, V. K. Vijay, R. Chandra and H. Kumar, *Clean. Eng. Technol.*, 2021, **3**, 100101.